Tests of general relativity at the fourth post-Newtonian order

Poulami Dutta Roy,[1,*] Sayantani Datta,[1,2,3] and K. G. Arun[1,3]

[1]*Chennai Mathematical Institute, Siruseri 603103, Tamil Nadu, India*
[2]*Department of Physics, University of Virginia, Charlottesville, Virginia 22904, USA*
[3]*Institute for Gravitation and the Cosmos, Department of Physics, Penn State University, University Park, Pennsylvania 16802, USA*

(Received 11 June 2024; accepted 30 July 2024; published 3 September 2024)

The recently computed post-Newtonian (PN) gravitational-wave phasing up to 4.5PN order accounts for several novel physical effects in compact binary dynamics such as the tail of the memory, tails of tails, and tails of mass hexadecapole and current octupole moments. Therefore, it is instructive to assess the ability of current-generation (2G) detectors such as LIGO and Virgo; next-generation (XG) ground-based gravitational wave detectors such as the Cosmic Explorer and Einstein Telescope; and space-based detectors like LISA to test the predictions of PN theory at these orders. Employing the Fisher information matrix, we find that the projected bounds on the deviations from the logarithmic PN phasing coefficient at 4PN are $\mathcal{O}(10^{-2})$ and $\mathcal{O}(10^{-1})$ for XG and 2G detectors, respectively. Similarly, the projected bounds on the other three PN coefficients that appear at 4PN and 4.5PN are $\mathcal{O}(10^{-1}$–$10^{-2})$ for XG and $\mathcal{O}(1)$ for 2G detectors. LISA observations of supermassive BHs could provide the tightest constraints on these four parameters in the range $\mathcal{O}(10^{-4}$–$10^{-2})$. The variation in these bounds is studied as a function of total mass and the mass ratio of the binaries in quasicircular orbits. These new tests are unique probes of higher order nonlinear interactions in compact binary dynamics and their consistency with the predictions of general relativity.

DOI: 10.1103/PhysRevD.110.064002

I. INTRODUCTION

The post-Newtonian (PN) approximation to general relativity (GR) has been very effective in modeling the compact binary dynamics during the adiabatic inspiral phase (see [1] for a comprehensive review). For nonspinning binaries in a quasicircular orbit, the contribution to the gravitational wave phase up to 3.5PN was computed using the multipolar post-Minkowskian formalism in Refs. [2–12]. The corresponding spin effects were computed in Refs. [13–33]. Recently, the gravitational wave (GW) flux and phasing for nonspinning compact binaries were extended up to 4.5PN, incorporating all nonlinear effects appearing till that order [34–53].

Therefore, it is pertinent to understand the importance of these newly computed terms in the context of testing GR using GWs, which is the theme of this paper.

Standard methods of testing GR in the inspiral regime include parametrized tests, which are routinely performed on the GW data [54–58]. These tests make the best use of our understanding of the compact binary dynamics in GR and introduce fractional deviation parameters at different PN orders in the GW phase [59–64]. The consistency of these fractional deformation parameters with zero is assessed by measuring them from observed signals and hence referred to as null tests. The resulting bounds from these theory-agnostic tests can be mapped to specific alternative theories of gravity as discussed, for example, in [65–71]. The parametrized tests are currently performed up to 3.5PN order in the inspiral phase. The newly computed 4PN and 4.5PN phasing corrections allow us to extend these tests and probe the novel physical effects that appear at such high PN orders, the neglect of which might result in systematic biases as shown in [72].

The precision of the parametrized tests will depend on the sensitivity of the GW detector. Proposed next-generation (XG) ground-based detectors such as the Cosmic Explorer (CE) [73] and Einstein Telescope (ET) [74,75] are capable of detecting compact binaries in the mass range up to a few hundreds of solar masses with a signal-to-noise ratio (SNR) of hundreds to thousands. Similarly, the planned Laser Interferometric Space Antenna (LISA) [76] can detect mergers of supermassive black holes that have masses of the order of several millions of solar masses, again, with SNRs of the order of thousands. Higher SNRs ensure better bounds on GR deviations. Various studies [77–82] have assessed the ability of these future detectors to carry out tests of GR. Therefore, along with the advanced LIGO (AdvLIGO) [83,84], advanced Virgo [85], KAGRA [86], GEO 600 [87], and LIGO-India [88,89], future GW

*Contact author: poulami@cmi.ac.in

detectors can test GR with unprecedented precision, which should be explored in the context of the new PN terms introduced in the inspiral phase.

A. Structure of the newly computed PN coefficients

The post-Newtonian theory is used to find an analytical expression of the inspiral GW phase in the slow-motion, weak-field regime when $v/c \ll 1$ and the binary constituents are sufficiently far away from each other. Within the framework of PN theory, in order to calculate the GW phase analytically, the binding energy (E) and GW flux ($\mathcal{F}$) emitted by the inspiraling binaries are expressed as a series in v/c, the structure of which, in geometrical units, can be schematically written as

$$E = -\frac{1}{2}\eta v^2 \sum_{k=0}^{N} E_k v^k, \qquad \mathcal{F} = \frac{32}{5}\eta^2 v^{10} \sum_{k=0}^{N} \mathcal{F}_k v^k, \tag{1}$$

where E_k and $\mathcal{F}_k$ are the PN expansion coefficients that appear in the energy and flux, respectively. For nonspinning binaries, these are functions of η, the symmetric mass ratio which is related to the mass ratio $q = \frac{m_1}{m_2}$ by $\eta = \frac{m_1 m_2}{(m_1+m_2)^2} = \frac{q}{(q+1)^2}$ (m_1 and m_2 denote the masses of the individual components of the binary). We will follow the convention $m_1 \geq m_2$ and $G = c = 1$ throughout the paper.

In the adiabatic approximation, the energy balance equation, $-dE/dt = \mathcal{F}$, in conjunction with the binding energy and flux functions introduced earlier, helps us compute the phase evolution $\Phi(t)$ of the GW signal. One can use the stationary phase approximation (SPA) [90,91] to perform the Fourier transform of the time domain gravitational wave signal and derive the phase (and amplitude) in the frequency domain for the ($\ell = 2$, $m = 2$) mode considered here with aligned spins. Until 3.5PN, this is a power series in v and $\ln v$, where $v = (\pi \mathrm{M} f)^{1/3}$ is the characteristic orbital velocity of the binary. The structure of the phase reads as

$$\Phi_{\rm insp}(f) = 2\pi f t_c - \phi_c + \frac{3}{128\eta v^5} \sum_{k=0}^{7} [\phi_k v^k + \phi_{{\rm k}\ell} v^k \ln v + \phi_{{\rm k}l^2} v^k \ln^2 v + \cdots]. \tag{2}$$

In the expression above, t_c and ϕ_c are two kinematical parameters that denote the time of coalescence and phase of coalescence. The leading order contribution (referred to as Newtonian or 0PN) corresponds to $k = 0$, and any term corresponding to v^k will be referred to as $\frac{k}{2}$ PN, in our notation.

Newly computed terms at 4PN and 4.5PN add to this structure. In order to highlight the structure of the new phasing terms, we rewrite Eq. (2) as

$$\Phi_{\rm insp}(f) = 2\pi f t_c - \phi_c + \frac{3}{128\eta v^5} [\phi_{\rm 3.5PN} + v^8(\phi_{8\ell} \ln v + \phi_{8\ell^2} \ln^2 v) + v^9(\phi_9 + \phi_{9\ell} \ln v)], \tag{3}$$

where $\phi_{\rm 3.5PN}$ denotes the 3.5PN phasing, normalized to the leading order Newtonian term, and the other terms denote the new PN coefficients at 4PN and 4.5PN orders. The explicit expressions of the PN coefficients $\phi_{8\ell}, \phi_{8\ell^2}, \phi_9$, and $\phi_{9\ell}$ can be found in [52,53]. Until 3.5PN, that is, $\mathcal{O}(v^7)$, the phasing in the frequency domain contains powers of v and two logarithmic terms at 2.5PN and 3PN. The logarithmic term at 2.5PN is not a generation effect (such a term does not appear in the GW flux) but a consequence of the SPA. The nonlogarithmic terms at 2.5PN can be reabsorbed into a redefinition of ϕ_c. The new terms at 4PN and 4.5PN bring two new logarithmic terms at 4PN and 4.5PN as well as a $\ln^2 v$ at 4PN, apart from a nonlogarithmic term at 4.5PN. There also exists a nonlogarithmic term at 4PN which can be absorbed into a redefinition of t_c. Apart from the nonspinning terms, starting at 1.5PN, the GW phasing contains spin effects like spin-orbit and spin-spin coupling along with tail-induced spin effects. Such effects are known completely for quasicircular orbits with nonprecessing spin until 3.5PN order [13–26]. At 4PN, the next-to-next-to-leading order contribution of the spin-spin interaction is also known [33]. We incorporate these spin effects in the inspiral phase up to 4PN order.

B. Physical effects at the new PN orders

Each PN order in phase carries signatures of various physical effects, which become more evident when the GW flux $\mathcal{F}$ [Eq. (1)] is expanded in terms of radiative multipole moments of the source [92] as

$$\mathcal{F} = \sum_{\ell \geq 2} [a_\ell U_L U_L + b_\ell V_L V_L], \tag{4}$$

where U_L and V_L denote multi-index symmetric trace-free tensors that represent the mass and current radiative multipole moments of the compact binary [see Eq. (2.1) in [53]] with a_ℓ and b_ℓ being numerical coefficients. Each PN term in flux would contain information about corresponding multipole moments up to certain PN orders [1,6–11,52]. For example, the computation of the flux at 4PN would require the knowledge of the mass quadrupole contribution U_{ij} computed till 4PN, mass octupole U_{ijk} and current quadrupole V_{ij} till 3PN, mass hexadecapole moment U_{ijkl} and current octupole V_{ijk} till 2PN, moments U_{ijklm}, V_{ijkl} at 1PN, and finally U_{ijklmn}, V_{ijklm} at Newtonian order. The relations between radiative multipoles and source multipoles contain several nonlinear effects of GR such as tails [4,6,93] and memory [94–96].

At 1.5PN in the flux, the GW "tail" effect first appears, corresponding to the quadratic interaction between the static ADM mass and the (source-type) mass quadrupole moment [4,6,93]. Physically, it denotes the backscattering of the quadrupolar GW by the spacetime curvature generated by the source's ADM mass. It is a "hereditary" effect due to its dependence on the entire history of the source until the retarded time. Similarly, at 2.5PN in the polarization, the "memory" effect appears [94–96], which corresponds to the quadrupole-quadrupole interaction (re-radiation of the stress-energy tensor). However, in the flux this is reduced to an instantaneous term due to the derivative operation. With increasing PN order, the complexity of the radiative moments increases as they contain higher order PN corrections to the existing effects as well as new nonlinear interactions, which have been studied in detail in the literature till 3.5PN [9,37,39,49,50,93,97,98].

At the newly computed 4PN order [52,53], two novel physical effects appear for the first time, namely, (i) "tail-of-memory" and (ii) "spin-quadrupole tail," both of which are hereditary effects. The tail-of-memory term denotes the scattering of re-radiated radiation by the background curvature of the source while the spin-quadrupole tail corresponds to the scattering of the radiation emitted from the spin-quadrupole interaction. A quartic interaction, dubbed "tails-of-tails-of-tails," occurs at 4.5PN order along with quartic memory interactions. Testing the agreement of such higher-order PN terms with GR provides a unique opportunity to quantify the consistency of novel physical effects occurring at these orders with the GW signal.

C. Parametrized tests of GR

The elegant structure of the PN phasing formula provides the perfect testing ground to probe the validity of GR through the parametrized tests [60,61,99]. These theory-agnostic tests of GR introduce normalized deviation parameters at each PN order of the inspiral phase. The coefficient at each PN order—ϕ_a where $a = \{\mathrm{k}, \mathrm{k}\ell, \mathrm{k}\ell^2\}$ and denote the nonlogarithmic, logarithmic, and square-logarithmic parts of the PN phase—is modified with a fractional deformation parameter $\delta\hat{\phi}_a$ ($\delta\hat{\phi}_{\mathrm{k}}$, $\delta\hat{\phi}_{\mathrm{k}\ell}$ and $\delta\hat{\phi}_{\mathrm{k}\ell^2}$) such that $\phi_a \to \phi_a^{\mathrm{GR}}(1 + \delta\hat{\phi}_a)$. By definition, $\delta\hat{\phi}_a = 0$ denotes GR, and if the posterior distribution of these parameters for a compact binary signal is consistent with zero, one would argue that the signal is statistically consistent with GR predictions. One can combine the information about these parameters from multiple events which, if GR is true, will help us place more stringent constraints than the individual events. The state-of-the-art bounds from deviations from GR for PN orders from −1PN until 3.5PN with LIGO/Virgo detectors can be found in Figs. 6 and 7 of [58].

In the spirit of the parametrized tests, we can introduce two null parameters each at 4PN and 4.5PN orders. At 4PN, there will be a logarithmic ($\delta\hat{\phi}_{8\ell}$) and logarithmic-square term ($\delta\hat{\phi}_{8\ell^2}$). At 4.5PN there is a nonlogarithmic term ($\delta\hat{\phi}_9$) and a logarithmic term ($\delta\hat{\phi}_{9\ell}$).

As the measurements of all of these parameters are accompanied by statistical uncertainties arising from the detector noise, we need to have a computationally inexpensive tool which can forecast the projected bounds on them in a reasonably reliable manner. The Fisher information matrix [91,100–103] provides such a semi-analytical tool which can estimate the projected bounds in the limit of sufficiently high SNR and is discussed in detail in Sec. III.

The future GW detectors, as discussed earlier, are expected to provide more stringent bounds on the deviation parameters due to their enhanced sensitivity and hence higher SNR. In this work, we employ the Fisher matrix to compute the bounds on the four new deviation parameters introduced at 4PN and 4.5PN using the noise power spectral densities (PSD) of the current (LIGO/Virgo) and XG GW (Cosmic Explorer, Einstein Telescope, and LISA) detectors.

A summary of our results can be found in Fig. 1 where we provide the projected bounds on the four new deformation parameters at 4PN and 4.5PN for the noise PSDs of AdvLIGO, CE, ET, and LISA. For the ground-based detectors, we choose GW150914-like and GW151226-like systems as shown in Fig. 1 while for LISA we consider a binary of mass $10^6 M_\odot$, mass ratio 1.2, and spins of magnitude (0.2, 0.1) at a luminosity distance of 3 Gpc. The 4PN log term $\delta\hat{\phi}_{8\ell}$ is seen to be best bounded irrespective of the detector, and all the deformation

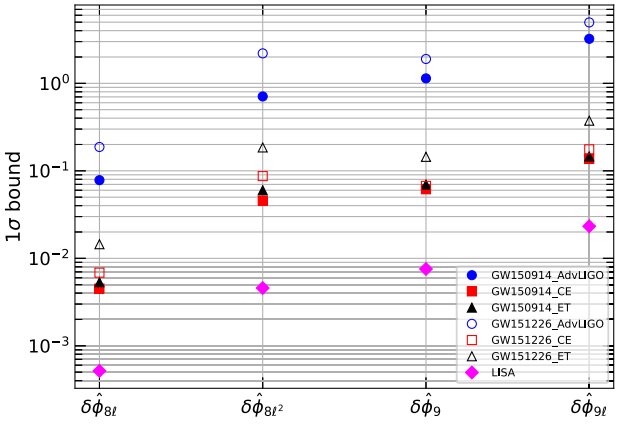

FIG. 1. Projected 1σ bounds on the four new deformation parameters introduced at 4PN and 4.5PN for a GW150914-like (at 440 Mpc) and GW151226-like (at 450 Mpc) system with the sensitivities of AdvLIGO, CE, and ET. Among ground-based detectors, CE/ET provides a tighter constraint than AdvLIGO for a particular system. Note that the bounds for a binary computed with CE and ET are comparable. The binary for LISA has total mass $10^6 M_\odot$, $q = 1.2$, and aligned spins of (0.2, 0.1) at 3 Gpc. The best bounds on parameters are obtained from supermassive binary black holes observed in LISA.

parameters have the best constraints from supermassive binary black holes observed in LISA. Note that the bounds projected with CE and ET sensitivities are comparable; thus, we consider CE as a representative of the XG detectors while computing bounds for most cases. However, it is known that ET has a lower cutoff frequency smaller than CE while CE has more sensitivity in the frequency band of 10 to 200 Hz. This trade-off might influence our results when studying the entire parameter range of BBH masses. Hence, we make a comparison of the bounds from CE and ET for certain parameter values to ensure that our conclusions remain consistent (see Fig. 3).

The remainder of the paper is organized as follows. In Sec. II, we briefly discuss the waveform model used in our analysis and the deformation coefficients introduced at 4PN and 4.5PN. Section III explains the formalism of the Fisher information matrix used to compute the 1σ bounds on the deformation coefficients. The main result obtained in our work, i.e., the bounds on the deformation parameters, are discussed in Sec. IV, followed by our conclusion in Sec. V. In the Appendix, we provide an assessment of how far the Fisher-based projections may be from the actual errors based on some representative binaries that have been detected and analyzed.

II. WAVEFORM MODEL

It is important to employ accurate waveform models for efficient and unbiased parameter inference. The advances in numerical relativity (NR) (see Ref. [104] for a review) have made it possible to construct phenomenological waveforms that include the inspiral and merger of binary compact objects, followed by the ringdown of the remnant formed. Such waveforms are often referred to as IMR waveforms. An important subclass of waveforms called IMRPhenom [105] was constructed to obtain a semi-analytical, computationally efficient waveform family suitable for GW searches and parameter estimation. Initially developed only for binaries with spins aligned with the orbital angular momentum vector [106,107], they were later modified to include precession [108,109] and higher modes [110].

As the real GW signals will have an inspiral, merger, and ringdown, our parametrization should be on the inspiral part of an IMR waveform to avoid any biases. For our purposes, we find it sufficient to use a non-precessing phenomenological family of waveforms called `IMRPhenomD` [106]. The `IMRPhenomD` waveform is based on a combination of analytic post-Newtonian and effective-one-body (EOB) methods describing the inspiral regime and calibration of the merger-ringdown model to numerical relativity simulations. Hence, it is easy to construct a parametrized IMR model where any of the PN coefficients are deformed from the GR value via the parametrization discussed earlier (see Sec. I C). As the detected population of compact binaries to date is dominantly nonprecessing [58], the projected bounds should still be representative of what may be achieved. A future work that assesses these bounds within the framework of Bayesian inference should employ more up-to-date waveforms with higher modes and precession effects such as `IMRPhenomXPHM` [109].

Schematically, the frequency-domain `IMRPhenomD` waveform can be written as

$$\tilde{h}(f) = \mathcal{A}(f) e^{i\Phi(f)}, \tag{5}$$

where $\mathcal{A}(f)$ and $\Phi(f)$ are the amplitude and phase of the waveform. The amplitude in the inspiral part agrees with the standard PN phase given in Eq. (2) up to 3.5PN order. We modify the inspiral segment of the `IMRPhenomD` waveform to incorporate the 4PN and 4.5PN phasing terms as described in Eq. (3). We also introduce the four new deformation parameters $\{\delta\hat{\phi}_{8\ell}, \delta\hat{\phi}_{8\ell^2}, \delta\hat{\phi}_{9}, \delta\hat{\phi}_{9\ell}\}$ in the inspiral phase of the waveform. We have removed the nonlogarithmic terms occurring at 2.5PN and 4PN as they can be absorbed in the redefinition of ϕ_c and t_c, respectively.

Ideally, the deformation parameters occurring at all PN orders should be measured simultaneously since any putative GR violation can occur at any PN order which is not known beforehand. However, due to the strong correlation among the deformation parameters themselves and also with the GR parameters, such multiparameter tests are uninformative, leading to poor estimation of the deviation parameters. Hence, one resorts to the obvious alternative of performing single-parameter tests where one deformation parameter is estimated at a time, along with other GR parameters of the binary. This has become a norm in tests of GR using gravitational waves. (See, for instance, Refs. [60,77–79,111–113] where multiparameter tests are discussed in detail).

In this work, we will also restrict ourselves to the standard practice of performing single-parameter tests where one of these deformation parameters is estimated along with all the GR parameters $\theta_{\rm GR} = \{\ln \mathrm{d_L}, \mathrm{t_c}, \phi_c, \ln \mathrm{M_c}, \eta, \chi_1, \chi_2\}$, where $\chi_{1,2}$ denote the dimensionless spin parameters of the binary components, $\mathrm{d_L}$ is the luminosity distance of the binary, and $\mathrm{M_c}$ is the chirp mass related to the total mass M by $\mathrm{M_c} = \mathrm{M}\eta^{3/5}$. Therefore, the $7+1$ dimensional parameter space consists of seven GR parameters and one deformation parameter.

Given the designed noise PSD of a GW detector, an estimate of the 1σ error bars associated with measuring these parameters can be obtained via the Fisher information matrix [91,103]. Since we are interested in studying the bounds on the PN deformation parameters and their correlation with the intrinsic parameters, we do not consider the effects of sky localization and orientations. The averaging over the source location and orientation results in a prefactor of $2/5$ multiplied to the amplitude of the

waveform [114,115] for the case of AdvLIGO, CE, and ET. To include the triangular shape of ET, a factor of $\sqrt{3}/2$ is multiplied to the waveform amplitude. On the other hand, the noise PSD of LISA already takes into account the 60° angle between the detector arms and the sky location and polarization averaging factors [79,116]. Hence, while computing the bounds for LISA, only a factor of $\sqrt{4/5}$ is multiplied to the amplitude of the `IMRPhenomD` waveform to account for the averaging over inclination angles.

III. ERROR ANALYSIS

Under the assumption of the detector noise being stationary and Gaussian, the distribution of various signal parameters can be approximated by a multivariate Gaussian described by the Fisher information matrix. In the limit of large SNRs, the 1σ widths provide lower limits on the statistical uncertainties associated with the measurement of the parameters usually referred to as the Cramer-Rao bound [100,101]. The Fisher information matrix is the noise weighted inner product of the derivatives of the frequency-domain waveform with respect to the eight parameters that we are concerned with here and evaluated at the true value of the parameters. Therefore, with the knowledge of the gravitational waveform of interest and the projected sensitivity of the detector, we can predict the measurement uncertainties of the parameters. There has been criticism of the use of the Fisher matrix for such projections, especially on signals that may have SNR $\mathcal{O}(10)$, which is the case for the LIGO and Virgo detectors [117]. However, if the problem at hand is to assess, at the order of magnitude level, the statistical uncertainties in the measurement, the Fisher matrix still provides a useful method to obtain them. More rigorous methods that numerically sample the likelihood functions may be used to quantify this more precisely as a future work. For instance, a recent work [118] carried out such a comparison in the context of XG detectors and argued that with an appropriate choice of priors, a Fisher matrix-based method can be employed for assessing the performance of XG detector configurations.

For different representative binary configurations, the Fisher matrix can be computed for a given detector PSD, which, in our case, is an 8×8 symmetric matrix, by construction. The inverse of the Fisher matrix is called the variance-covariance matrix. The square root of the diagonal entries of this matrix gives a 1σ error bar, which is of interest to us. More precisely, the Fisher matrix is defined as

$$\Gamma_{ab} = 2\int_{f_{\rm low}}^{f_{\rm up}} \frac{\tilde{h}_{,a}\tilde{h}^{*}_{,b} + \tilde{h}_{,b}\tilde{h}^{*}_{,a}}{S_n(f)}\,df, \tag{6}$$

where commas denote partial differentiation of the waveform with respect to various parameters θ^a and the asterisks denote complex conjugation. The tilde denotes the Fourier transform of the time domain signal $h(t)$, and $S_n(f)$ is the noise PSD of the detector of interest.

In this work, we study three representative detector configurations: AdvLIGO as the representative of the second-generation GW detector,[1] and the Cosmic Explorer and LISA as representatives of the ground-based and space-based next-generation detectors, respectively. We use the designed noise PSD of Advanced LIGO, given in Eq. (4.7) of [119], the CE PSD given in [120], the ET PSD in [121], and the LISA noise PSD discussed in [79,116]. The LISA noise PSD has two distinct contributions, one from the instrument noise and another from the galactic confusion noise. The instrumental noise PSD given in [116] is divided by a factor of 2 to account for summation over two independent frequency channels. On the other hand, the unresolved galactic binaries contribute to a background confusion noise in the low-frequency regime, $f \lesssim 1$ mHz, which is modeled through an analytical expression given in [122] for a four-year observation period of LISA.

The SNR quantifies the strength of the signal in detector data. The SNR denoted by ρ is defined using the Fourier transform of the signal $\tilde{h}(f)$, as

$$\rho^2 = 4\int_{f_{\rm low}}^{f_{\rm up}} \frac{|\tilde{h}(f)|^2}{S_n(f)}\,df. \tag{7}$$

The lower cutoff frequency, for ground-based detectors, in the Fisher analysis depends on the detector, $f_{\rm low} =$ 10 Hz for AdvLIGO, 5 Hz for CE, and 1 Hz for ET. The upper cutoff frequency, on the other hand, is formally infinity. However, following Ref. [112], we set $f_{\rm up} = f_{\rm IMR}$ where $f_{\rm IMR}$ corresponds to the frequency at which the characteristic amplitude $2\sqrt{f}|\tilde{h}(f)|$ of the GW signal is lower than that of the detector noise amplitude spectral density by 10% at maximum. For binaries of mass $10-110M_\odot$ at a luminosity distance of 500 Mpc, the SNR for different mass ratios varies from ∼10–50 for AdvLIGO, and for CE with masses ∼10–$600M_\odot$, the SNR varies from $\sim 10^2$–10^4. For AdvLIGO, certain mass choices, like the total mass of $10M_\odot$ with any mass ratio, have SNR < 10 and are excluded from our analysis.

Since the sensitivity of LISA will allow the observation of GW signals from supermassive black holes, we select the mass range of the binary to be 10^4–$10^7M_\odot$ while keeping the mass ratios the same as those used for the ground-based detectors. LISA is sensitive in the mHz frequency regime, with lower and upper cutoff frequencies decided by the binary parameters. The lower cutoff frequency is chosen such that the GW signal from the inspiraling binary lasts for four years prior to its merger but is not lower than the

[1]As the designed sensitivity of Virgo is similar to that of LIGO, we use LIGO as a proxy for Virgo and any other detectors that have similar sensitivity.

low-frequency limit of the LISA noise PSD, which is 10^{-4} Hz. Hence, the lower cutoff frequency is chosen as [79,123]

$$f_{\rm low} = {\rm Max}\left[10^{-4}, 4.149\times10^{-5}\left(\frac{M_c}{10^6}\right)^{-5/8} T_{\rm obs}^{-3/8}\right], \quad (8)$$

where $T_{\rm obs}$ is the duration of the observation of LISA, i.e., four years, and M_c is the chirp mass in solar mass units. The upper cutoff frequency is chosen between $f_{\rm IMR}$ and the upper frequency limit of 0.1 Hz, whichever is smaller,

$$f_{\rm up} = {\rm Min}[f_{\rm IMR}, 0.1]. \quad (9)$$

The supermassive black hole binaries at 3 Gpc luminosity distance have SNR in LISA in the range $\sim 10^2$–10^4 for different masses and mass ratios.

In our analysis, we also incorporate the effect of redshift in the observed masses of the compact binaries through a factor of $1+z$, where z is the redshift of the source. In other words, the detector-frame masses $m_{\rm det}$ are related to the source-frame masses of the binary m_s as $m_{\rm det} = m_s(1+z)$. Throughout the paper, we refer to the source-frame masses of the binaries unless specified otherwise. For a fixed luminosity distance, we assume the flat Λ-CDM model and calculate the associated redshift z by employing

$$d_L(z) = \frac{(1+z)}{H_0}\int_0^z \frac{dz'}{\sqrt{\Omega_M(1+z')^3+\Omega_\Lambda}}, \quad (10)$$

where the cosmological parameters are $\Omega_M = 0.3065$, $\Omega_\Lambda = 0.6935$, and $h = 0.6790$ with $H_0 = 100h$ (km/s)/Mpc [124]. In the Fisher matrix code, the assumed luminosity distance of the source is used to obtain the redshift of the source and hence the redshifted mass.

IV. RESULTS

A. Projected bounds on events like GW150914 and GW151226

In this section, we show the projected bounds on all the deformation parameters from 0PN to 4.5PN with AdvLIGO sensitivity for binary black holes having parameters similar to GW150914 [125] and GW151226 [126], the first two detections made by LIGO during the first observing run. On the one hand, these two events represent two interesting regimes of the dynamics. GW150914 is a relatively high mass system for which we observe only a few cycles of late inspiral whereas GW151226 has several cycles of inspiral in the frequency bands of LIGO/Virgo. This also helps us understand how the errors vary as a function of PN order. As the LIGO-Virgo-KAGRA (LVK) Collaboration analyses usually quote 90% credible bounds, we convert the 1σ bounds from the Fisher matrix to 90% credibility. The parameters of the binaries are taken from the median values of the LVK posteriors, including those of the luminosity distances (see Table III of [127]).

TABLE I. Projected Fisher 90% bound obtained for GW150914-like (at 440 Mpc) and GW151226-like (at 450 Mpc) binary masses and spins with AdvLIGO sensitivity having SNRs of 39.8 and 16.2, respectively. We use our modified waveform, which includes all deformation parameters till 4.5PN.

$\delta\hat{\phi}_k$	GW150914-like	GW151226-like
$\delta\hat{\phi}_0$	0.05	0.18
$\delta\hat{\phi}_2$	0.11	0.14
$\delta\hat{\phi}_3$	0.06	0.13
$\delta\hat{\phi}_4$	0.41	1.21
$\delta\hat{\phi}_{5\ell}$	0.13	0.35
$\delta\hat{\phi}_6$	0.25	0.92
$\delta\hat{\phi}_{6\ell}$	0.98	2.34
$\delta\hat{\phi}_7$	0.50	1.46
$\delta\hat{\phi}_{8\ell}$	0.13	0.31
$\delta\hat{\phi}_{8\ell^2}$	1.16	3.63
$\delta\hat{\phi}_9$	1.87	3.12
$\delta\hat{\phi}_{9\ell}$	5.31	8.17

The projected bound on the 12 deformation parameters for AdvLIGO-like sensitivity are shown in Table I for these two binaries. The variation of the bounds across PN orders does not show any monotonic trends. Parameters at higher PN orders are not necessarily more poorly constrained than some of the lower PN order parameters. This is due to the well-known oscillatory convergence of the PN series and has been observed in various data analysis contexts (see, for example, Table 1 of Ref. [59]). The trends until 3.5PN can be compared against the trends reported by LVK in Fig. 4 of [56] from the analysis of the two above-mentioned GW events. We find that these two trends match exactly. We cannot compare the bounds themselves here as, apart from using the Fisher matrix for the projections, the noise PSDs we use are those of the designed sensitivity of AdvLIGO, whereas [56] uses the sensitivity of LIGO and Virgo during the first observing run when these two events were detected. Precisely due to this reason, our bounds are better than those in [56]. Next, looking at the bounds on the new parameters that appear at 4PN and 4.5PN orders, we find that, with the exception of $\delta\hat{\phi}_{8\ell}$, the other three parameters are likely to yield poorer constraints than all the parameters till 3.5PN.

B. Variation of the bounds as a function of binary parameters

We now compute the projected bounds on $\{\delta\hat{\phi}_{8\ell}, \delta\hat{\phi}_{8\ell^2}, \delta\hat{\phi}_9, \delta\hat{\phi}_{9\ell}\}$ and their variation as a function of total mass and mass ratios of the binaries for current-generation detectors (represented by AdvLIGO), next-generation ground-based detectors (represented by CE), and the

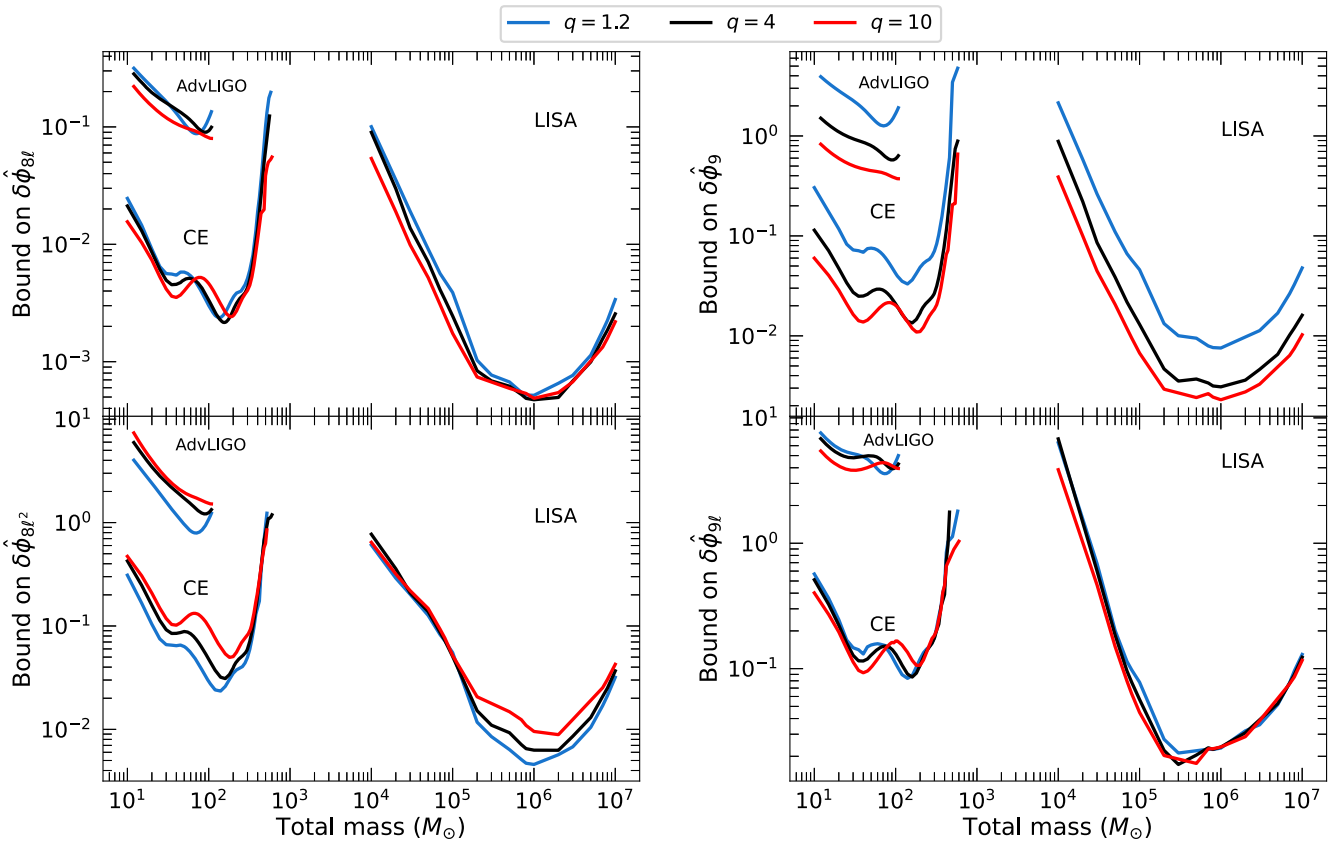

FIG. 2. Projected 1σ bounds on the deformation parameters corresponding to the 4PN and 4.5PN phasing terms for AdvLIGO, CE, and LISA sensitivities. Different total mass binaries are considered with mass ratios $q = 1.2$, 4, 10 and aligned spin $\chi_{1,2} = (0.2, 0.1)$. The sources are at a luminosity distance of 500 Mpc ($z = 0.1049$) for AdvLIGO/CE and at 3 Gpc ($z = 0.512$) for LISA.

space-based LISA detector; we analyze masses from a few solar masses to $10^7 M_\odot$. Since our work focuses on constraining these deformation parameters associated with the nonspinning part of the inspiral phase, we keep the magnitudes of the aligned binary spins fixed in our analysis. The spins are chosen to be (0.2, 0.1), which is consistent with the fact that the observed BBH population has relatively smaller component spins [58]. The variation in spin magnitude is not expected to alter the trends shown by the bounds significantly. A detailed quantification of this will be addressed in a future work.

1. Advanced LIGO and Cosmic Explorer results

We focus on the bounds of the deformation parameters from ground-based detectors in this section. We consider the binaries to be at 500 Mpc ($z = 0.1049$), having spin magnitudes (0.2, 0.1) aligned with the orbital angular momentum. The total mass is varied from $10 - 110 M_\odot$ for AdvLIGO and from $10 - 600 M_\odot$ for CE. There is very little inspiral in the bands of the respective detectors beyond these mass ranges; hence, binaries with masses after this maximum mass are unsuitable for our tests. For a particular total mass, we study systems with different mass ratios $q = 1.2$, 4, 10. Figure 2 shows the 1σ bound on the deformation parameters as a function of the total mass of the binary for different q for both AdvLIGO and CE.

Initially, we observe a gradual improvement in the bound of the parameters with increasing total mass, for all detectors, which can be attributed to increasing SNR for high-mass systems. But as the total mass increases, the signal has a lower number of cycles in band, as the merger frequency is inversely proportional to the mass. This leads to a degradation of the bounds after some total mass depending on the detector PSD. Of the four deformation parameters, $\delta\hat{\phi}_{8\ell}$ has the best bound, with a precision of $\sim 10^{-1}(10^{-3})$ for AdvLIGO (CE). Further, we find that CE can constrain $\delta\hat{\phi}_9$ by $\sim 10^{-2}$ and the remaining deformation parameters by $\sim 10^{-1}$. Typical numbers for representative systems (GW150914-like and GW151226-like) are also shown in Fig. 1. We observe that, once again in Fig. 1, the higher mass binary corresponding to GW150914 gives a better bound on the parameters than GW151226, with $\delta\hat{\phi}_{8\ell}$ being the best measured. Figure 2 shows that the bounds on $\delta\hat{\phi}_{8\ell}$, $\delta\hat{\phi}_9$, and $\delta\hat{\phi}_{9\ell}$ improve for more asymmetric binaries or systems that have larger mass ratios. This is because the PN coefficients corresponding to these three terms are dominated by the nonquadrupolar modes [52,53] which are strongly excited for the asymmetric systems, hence leading

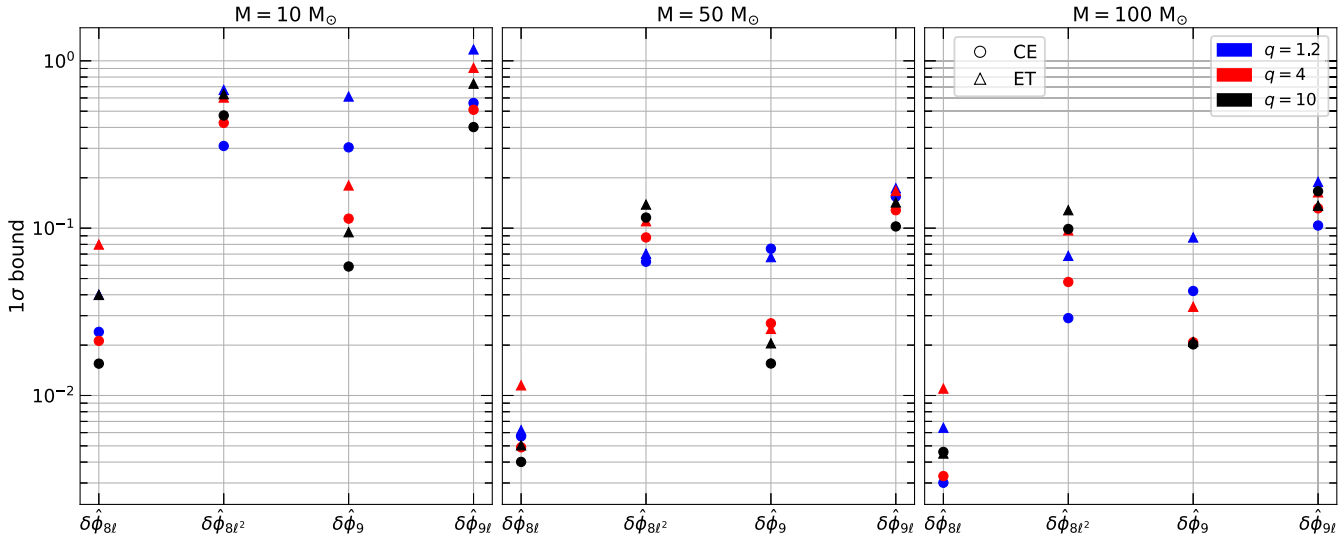

FIG. 3. Projected 1σ bounds on the deformation parameters corresponding to the 4PN and 4.5PN phasing terms for CE and ET sensitivities. Binaries of total mass 10, 50, and $100M_\odot$ are considered as representatives with mass ratios $q = 1.2, 4, 10$ and aligned spin $\chi_{1,2} = (0.2, 0.1)$. The sources are at a luminosity distance of 500 Mpc ($z = 0.1049$). Bounds from CE and ET are comparable for higher mass binaries while CE performs better for low mass cases.

to better bounds for asymmetric binaries. On the other hand, bounds on $\delta\hat{\phi}_{8\ell^2}$ are the best when the binary is more symmetric. Upon examining the multipoles that contribute to the 4PN log-square term, it is evident that quadrupole moments occurring at different PN orders dominantly contribute to this order, hence giving better bounds for symmetric binaries.

Finally, it is seen from the plots that with the exception of $\delta\hat{\phi}_{9\ell}$, parameters at 4PN and 4.5PN can yield bounds $\leq \mathcal{O}(1)$, even with AdvLIGO sensitivity for an appropriate ranges of mass and mass ratios, presenting a unique opportunity to test the validity of GR at such high PN orders, even with LIGO. The magnitude of the bound improves significantly for CE due to its enhanced sensitivity.

Since the bounds in Fig. 2 are computed only with CE sensitivity for the case of 3G detectors, we compute the bounds for ET as well for certain representative masses and compare them with CE. In Fig. 3, we show bounds obtained from both CE and ET for 10, 50, and $100M_\odot$ and varying mass ratios. We observe that with increasing total mass, the projected bounds from the two detectors become comparable due to the lower number of inspiral cycles. On the other hand, for $10M_\odot$, CE performs slightly better since the sensitivity of CE is better in the midfrequency range than ET where the majority of the inspiral cycles fall. Overall, the conclusions obtained from Fig. 2 still hold when ET is included in the analysis.

2. Results for LISA

In the previous section, we observed that the four new deformation parameters at 4PN and 4.5PN can be bounded reasonably with AdvLIGO and CE sensitivity. The total masses of the binaries that yield the best bounds are $\sim 100M_\odot$. On the other hand, the space-based detector LISA will observe the merger of supermassive black hole binaries with masses of $\sim 10^4$–$10^7 M_\odot$. In this section, we will estimate the projected bounds on $\{\delta\hat{\phi}_{8\ell}, \delta\hat{\phi}_{8\ell^2}, \delta\hat{\phi}_9, \delta\hat{\phi}_{9\ell}\}$ from the GW signals of supermassive black hole binary mergers that will be detected by LISA. The total mass of the binaries is varied in the range 10^4–$10^7 M_\odot$, and the mass ratios are $q = 1.2, 4, 10$. We consider the binaries at a prototypical luminosity distance of 3 Gpc ($z = 0.512$), with spin magnitudes (0.2, 0.1) aligned with the orbital angular momentum. Figure 2 shows our LISA results.

The dependence of the bounds on the mass ratios is qualitatively the same as observed for AdvLIGO/CE. Similar to the case of AdvLIGO/CE, the best bounds on the parameter $\delta\hat{\phi}_{8\ell^2}$ are for the more symmetric binaries with $q = 1.2$. The remaining three parameters are better constrained for more asymmetric systems. The parameter $\delta\hat{\phi}_{8\ell}$, once again, has the best bound of $\sim 10^{-3}$ while $\{\delta\hat{\phi}_{8\ell^2}, \delta\hat{\phi}_9\}$ have bounds of $\sim 10^{-2}$ and, finally, $\delta\hat{\phi}_{9\ell}$ has the worst bound of $\sim 10^{-1}$. Hence, we find that the four deformation parameters can be constrained to a very good precision with GWs from supermassive binary black holes, as observed by LISA. These bounds clearly outsmart the bounds from CE, thanks to the longer duration of the signals in the LISA band.

V. CONCLUSION

The parametrized tests of GR with the inspiral dynamics are currently performed using the expansion of the inspiral

phase up to 3.5PN. The recent analytical computation of terms occurring at 4PN and 4.5PN of the inspiral phase for quasicircular, nonspinning binaries allows us to extend these tests to 4.5PN. The four new PN coefficients that occur at 4PN and 4.5PN permit tests of novel physical effects such as the tail-of-memory, spin-quadrupole tails, and quartic tails. In this work, we compute the projected 1σ bounds on the four new deformation coefficients, $\{\delta\hat{\phi}_{8\ell}, \delta\hat{\phi}_{8\ell^2}, \delta\hat{\phi}_9, \delta\hat{\phi}_{9\ell}\}$, which are introduced in the logarithmic, square-logarithmic, and nonlogarithmic terms appearing at 4PN and 4.5PN. We employ the Fisher analysis with a modified `IMRPhenomD` waveform for estimating the bounds. For different binary configurations and detectors (AdvLIGO, CE, and LISA), the bounds are shown in Fig. 2, and the main results are summarized as follows.

The parameter corresponding to the 4PN log term, $\delta\hat{\phi}_{8\ell}$, has the best bound of $\sim 10^{-3}$ from LISA, $\sim 10^{-2}$ from CE, and $\sim 10^{-1}$ from AdvLIGO. For the remaining three deformation parameters, the bounds are $\mathcal{O}(10^{-2} - 1)$ for CE and $\leq \mathcal{O}(10)$ for AdvLIGO. The best constraint for all the parameters are obtained from supermassive binary black holes observed in LISA due to the longer duration of the inspiral signal seen in this band.

The network of 3G detectors will observe orders of magnitude more sources compared to the current-generation detectors. This allows one to combine the bounds from these events. One can do this either by multiplying the respective likelihoods (assuming the deformation parameter takes the same value across all events) [128,129] or hierarchically combine the posteriors, allowing the deformation parameter to be different across events [58,130,131]. For Gaussian noise, when multiplying the likelihoods, the statistical error decreases as $\sim 1/\sqrt{N}$, where N is the number of events detected, and the bounds are expected to improve when combining results from multiple events. Assuming a network of 3G detectors, consisting of two CE with arm lengths of 40 km and 20 km and one ET, $N \sim 6 \times 10^4$ BBH events with SNR greater than 30 are expected to be observed per year [132]. With these estimates, the bounds on the 4PN log term, say, will improve from $\mathcal{O}(10^{-2})$ to $\mathcal{O}(10^{-5})$ for 3G. Similar estimations for LISA are difficult due to the uncertainties related to the detection rates of SMBBH mergers by LISA. Finally, we conclude that apart from $\delta\hat{\phi}_{9\ell}$, deviation from GR at 4PN and 4.5PN can be constrained with $\leq \mathcal{O}(1)$ precision even with AdvLIGO sensitivity, presenting a unique possibility to utilize the rich character of the inspiral phase in the high-frequency regime to study GR violation.

All these projections are based on the Fisher matrix formalism and are valid when the SNRs are sufficiently high. In order to assess the error bars on our projections, we compare the bounds from the parametrized tests performed for GW150914 and GW151226 with what our approach would have predicted for the same. The results are given in Table II, and details of the comparison are given in the Appendix. For the inspiral-dominated GW151226, our projections are found to underestimate the true bounds by up to a factor of 2. This underestimation can be up to a factor of 4 (or even 8 for a 2.5PN logarithmic parameter) in the case of the more massive GW150914. Therefore, a more detailed Bayesian analysis with waveforms having precession and higher modes will be the next step to support the bounds from the Fisher analysis and will be pursued in future projects.

TABLE II. Comparison of 90% bounds on deformation parameters using O1 noise PSD and the `IMRPhenomD` waveform till 3.5PN for GW150914 and GW151226. We have taken the values of the binary mass, mass ratio, spin, and luminosity distance for the events, as quoted in Table III of [127]. The Fisher matrix bound is normalized with the network SNR corresponding to these events.

Event	PN	LVK	Fisher 90% bound	LVK/Fisher
GW150914	0	0.2	0.07	2.57
SNR = 16.311	1	0.6	0.21	2.88
LVK SNR = 25.3	1.5	0.4	0.12	3.39
	2	3	0.61	4.94
	2.5 l	1.5	0.18	8.23
	3	2	1.07	1.85
	3 l	10.5	4.13	2.54
	3.5	5.5	3.05	1.79
GW151226	0	0.2	0.13	1.55
SNR = 6.38	1	0.3	0.23	1.33
LVK SNR = 12.4	1.5	0.2	0.14	1.39
	2	1.8	1.09	1.65
	2.5l	0.6	0.37	1.61
	3	1.5	1.19	1.61
	3l	7	4.16	1.68
	3.5	4	2.28	1.74

ACKNOWLEDGMENTS

We would like to thank Sebastian Khan for sharing his *Mathematica* code of the IMRPhenomD waveform model with us. We thank N. V. Krishnendu for useful comments on the manuscript. We also thank Pankaj Saini and Parthapratim Mahapatra for useful discussions. K. G. A. acknowledges support from Swarnajayanti Fellowship Grant No. DST/SJF/PSA-01/2017-18 and Core Research Grant No. CRG/2021/004565 of the SERB. K. G. A and P. D. R. acknowledge support from the Infosys Foundation. S. D. acknowledges support from the UVA Arts and Sciences Rising Scholars Fellowship. This material is based upon work supported by NSF's LIGO Laboratory, which is a major facility fully funded by the National Science Foundation.

APPENDIX: COMPARISON OF FISHER-BASED BOUNDS WITH EXISTING LVK RESULTS

The Fisher matrix projections are expected to be reliable only for high SNR systems. In this Appendix, we will compare the bounds on the deviation parameters, till 3.5PN, computed through the Fisher matrix with those obtained from Bayesian analysis to estimate the accuracy of our predicted bounds for the new deformation parameters. More specifically, we compare the Fisher-based 90% bound with the values obtained by LVK in the events catalogued in GWTC-1 [127]. We take $f_{\rm low} = 20$ Hz, with the upper limit of frequency being $f_{\rm IMR}$ (see Sec. III). The 1σ bounds obtained from the Fisher analysis are converted to those at 90% credibility. We use the O1 noise PSD and normalize the Fisher matrix bound with respect to the network SNR corresponding to a particular event. We approximate the $\chi_{1,2}$ values by the median $\chi_{\rm eff}$ value quoted in [127]. Likewise, we consider the corresponding median values for the mass and luminosity distance of the binaries. The last column in Table II shows the LVK-to-Fisher bound ratio, which, if equal to 1, denotes the exact match between the bounds from the two methods. We find that the Fisher-based bounds are comparable with the Bayesian bounds, at least for GW151226, which is inspiral dominated. Even for heavy mass binaries like GW150914, apart from the 2.5PN log term, the constraints on the other PN order deformation parameters differ from the LVK bound by a factor of $\sim$1 to 4.

[1] L. Blanchet, Living Rev. Relativity **17**, 2 (2014).
[2] L. Blanchet and T. Damour, Ann. Inst. Henri Poincaré Phys. Théor. **50**, 377 (1989), http://www.numdam.org/item/?id=AIHPA_1989__50_4_377_0.
[3] W. Junker and G. Schäfer, Mon. Not. R. Astron. Soc **254**, 146 (1992).
[4] L. Blanchet and G. Schäfer, Classical Quantum Gravity **10**, 2699 (1993).
[5] L. Blanchet, T. Damour, B. R. Iyer, C. M. Will, and A. G. Wiseman, Phys. Rev. Lett. **74**, 3515 (1995).
[6] L. Blanchet, T. Damour, and B. R. Iyer, Phys. Rev. D **51**, 5360 (1995); **54**, 1860(E) (1996).
[7] L. Blanchet, B. R. Iyer, C. M. Will, and A. G. Wiseman, Classical Quantum Gravity **13**, 575 (1996).
[8] L. Blanchet, Phys. Rev. D **54**, 1417 (1996); **71**, 129904(E) (2005).
[9] L. Blanchet, Classical Quantum Gravity **15**, 113 (1998); **22**, 3381(E) (2005).
[10] L. Blanchet, B. R. Iyer, and B. Joguet, Phys. Rev. D **65**, 064005 (2002); **71**, 129903(E) (2005).
[11] L. Blanchet, G. Faye, B. R. Iyer, and B. Joguet, Phys. Rev. D **65**, 061501 (2002); **71**, 129902(E) (2005).
[12] L. Blanchet, T. Damour, G. Esposito-Farese, and B. R. Iyer, Phys. Rev. Lett. **93**, 091101 (2004).
[13] L. Kidder, C. Will, and A. Wiseman, Phys. Rev. D **47**, R4183 (1993).
[14] L. E. Kidder, Phys. Rev. D **52**, 821 (1995).
[15] G. Faye, L. Blanchet, and A. Buonanno, Phys. Rev. D **74**, 104033 (2006).
[16] L. Blanchet, A. Buonanno, and G. Faye, Phys. Rev. D **74**, 104034 (2006); **75**, 049903(E) (2007); **81**, 089901(E) (2010).
[17] K. G. Arun, A. Buonanno, G. Faye, and E. Ochsner, Phys. Rev. D **79**, 104023 (2009); **84**, 049901(E) (2011).
[18] L. Blanchet, A. Buonanno, and G. Faye, Phys. Rev. D **84**, 064041 (2011).
[19] S. Marsat, A. Bohe, G. Faye, and L. Blanchet, Classical Quantum Gravity **30**, 055007 (2013).
[20] A. Buonanno, G. Faye, and T. Hinderer, Phys. Rev. D **87**, 044009 (2013).
[21] S. Marsat, A. BohÈ, L. Blanchet, and A. Buonanno, Classical Quantum Gravity **31**, 025023 (2014).
[22] A. BohÈ, S. Marsat, and L. Blanchet, Classical Quantum Gravity **30**, 135009 (2013).
[23] S. Marsat, Classical Quantum Gravity **32**, 085008 (2015).
[24] A. Bohé, G. Faye, S. Marsat, and E. K. Porter, Classical Quantum Gravity **32**, 195010 (2015).
[25] C. K. Mishra, A. Kela, K. G. Arun, and G. Faye, Phys. Rev. D **93**, 084054 (2016).
[26] Q. Henry, S. Marsat, and M. Khalil, Phys. Rev. D **106**, 124018 (2022).
[27] R. A. Porto, Phys. Rev. D **73**, 104031 (2006).
[28] R. A. Porto and I. Z. Rothstein, Phys. Rev. D **78**, 044012 (2008); **81**, 029904(E) (2010).
[29] R. A. Porto and I. Z. Rothstein, Phys. Rev. D **78**, 044013 (2008); **81**, 029905(E) (2010).
[30] N. T. Maia, C. R. Galley, A. K. Leibovich, and R. A. Porto, Phys. Rev. D **96**, 084065 (2017).
[31] N. T. Maia, C. R. Galley, A. K. Leibovich, and R. A. Porto, Phys. Rev. D **96**, 084064 (2017).
[32] G. Cho, B. Pardo, and R. A. Porto, Phys. Rev. D **104**, 024037 (2021).
[33] G. Cho, R. A. Porto, and Z. Yang, Phys. Rev. D **106**, L101501 (2022).
[34] S. Foffa and R. Sturani, Phys. Rev. D **87**, 044056 (2013).
[35] S. Foffa and R. Sturani, Phys. Rev. D **87**, 064011 (2013).
[36] D. Bini and T. Damour, Phys. Rev. D **87**, 121501 (2013).
[37] G. Faye, L. Blanchet, and B. R. Iyer, Classical Quantum Gravity **32**, 045016 (2015).
[38] C. R. Galley, A. K. Leibovich, R. A. Porto, and A. Ross, Phys. Rev. D **93**, 124010 (2016).
[39] T. Marchand, L. Blanchet, and G. Faye, Classical Quantum Gravity **33**, 244003 (2016).
[40] S. Foffa, P. Mastrolia, R. Sturani, and C. Sturm, Phys. Rev. D **95**, 104009 (2017).

[41] R. A. Porto and I. Z. Rothstein, Phys. Rev. D **96**, 024062 (2017).
[42] S. Foffa and R. Sturani, Phys. Rev. D **100**, 024047 (2019).
[43] S. Foffa, R. A. Porto, I. Rothstein, and R. Sturani, Phys. Rev. D **100**, 024048 (2019).
[44] J. Blümlein, A. Maier, P. Marquard, and G. Schäfer, Nucl. Phys. **B955**, 115041 (2020).
[45] T. Marchand, Q. Henry, F. Larrouturou, S. Marsat, G. Faye, and L. Blanchet, Classical Quantum Gravity **37**, 215006 (2020).
[46] F. Larrouturou, Q. Henry, L. Blanchet, and G. Faye, Classical Quantum Gravity **39**, 115007 (2022).
[47] F. Larrouturou, L. Blanchet, Q. Henry, and G. Faye, Classical Quantum Gravity **39**, 115008 (2022).
[48] Q. Henry, G. Faye, and L. Blanchet, Classical Quantum Gravity **38**, 185004 (2021).
[49] D. Trestini and L. Blanchet, Phys. Rev. D **107**, 104048 (2023).
[50] L. Blanchet, G. Faye, and F. Larrouturou, Classical Quantum Gravity **39**, 195003 (2022).
[51] D. Trestini, F. Larrouturou, and L. Blanchet, Classical Quantum Gravity **40**, 055006 (2023).
[52] L. Blanchet, G. Faye, Q. Henry, F. m. c. Larrouturou, and D. Trestini, Phys. Rev. Lett. **131**, 121402 (2023).
[53] L. Blanchet, G. Faye, Q. Henry, F. m. c. Larrouturou, and D. Trestini, Phys. Rev. D **108**, 064041 (2023).
[54] B. P. Abbott *et al.* (LIGO Scientific and Virgo Collaborations), Phys. Rev. Lett. **116**, 221101 (2016); **121**, 129902(E) (2018).
[55] B. P. Abbott *et al.* (LIGO Scientific and Virgo Collaborations), Phys. Rev. Lett. **123**, 011102 (2019).
[56] B. P. Abbott *et al.* (LIGO Scientific and Virgo Collaborations), Phys. Rev. D **100**, 104036 (2019).
[57] R. Abbott *et al.* (LIGO Scientific and Virgo Collaborations), Phys. Rev. D **103**, 122002 (2021).
[58] R. Abbott *et al.* (LIGO Scientific, Virgo, and KAGRA Collaborations), arXiv:2112.06861.
[59] K. G. Arun, B. R. Iyer, B. S. Sathyaprakash, and P. A. Sundararajan, Phys. Rev. D **71**, 084008 (2005); **72**, 069903(E) (2005).
[60] K. G. Arun, B. R. Iyer, M. S. S. Qusailah, and B. S. Sathyaprakash, Classical Quantum Gravity **23**, L37 (2006).
[61] K. G. Arun, B. R. Iyer, M. S. S. Qusailah, and B. S. Sathyaprakash, Phys. Rev. D **74**, 024006 (2006).
[62] N. Cornish, L. Sampson, N. Yunes, and F. Pretorius, Phys. Rev. D **84**, 062003 (2011).
[63] M. Agathos, W. Del Pozzo, T. G. F. Li, C. Van Den Broeck, J. Veitch, and S. Vitale, Phys. Rev. D **89**, 082001 (2014).
[64] A. K. Mehta, A. Buonanno, R. Cotesta, A. Ghosh, N. Sennett, and J. Steinhoff, Phys. Rev. D **107**, 044020 (2023).
[65] K. Yagi, L. C. Stein, N. Yunes, and T. Tanaka, Phys. Rev. D **85**, 064022 (2012); **93**, 029902(E) (2016).
[66] K. Yagi, N. Yunes, and T. Tanaka, Phys. Rev. Lett. **109**, 251105 (2012).
[67] N. Yunes, P. Pani, and V. Cardoso, Phys. Rev. D **85**, 102003 (2012).
[68] K. Yagi, N. Yunes, and T. Tanaka, Phys. Rev. D **86**, 044037 (2012); **89**, 049902(E) (2014).
[69] N. Yunes and X. Siemens, Living Rev. Relativity **16**, 9 (2013).
[70] L. Sampson, N. Yunes, N. Cornish, M. Ponce, E. Barausse, A. Klein, C. Palenzuela, and L. Lehner, Phys. Rev. D **90**, 124091 (2014).
[71] N. Yunes, K. Yagi, and F. Pretorius, Phys. Rev. D **94**, 084002 (2016).
[72] C. B. Owen, C.-J. Haster, S. Perkins, N. J. Cornish, and N. Yunes, Phys. Rev. D **108**, 044018 (2023).
[73] D. Reitze *et al.*, Bull. Am. Astron. Soc. **51**, 035 (2019), arXiv:1907.04833.
[74] M. Punturo *et al.*, Classical Quantum Gravity **27**, 194002 (2010).
[75] M. Maggiore *et al.*, J. Cosmol. Astropart. Phys. 03 (2020) 050.
[76] P. Amaro-Seoane *et al.* (LISA Collaboration), arXiv:1702.00786.
[77] A. Gupta, S. Datta, S. Kastha, S. Borhanian, K. G. Arun, and B. S. Sathyaprakash, Phys. Rev. Lett. **125**, 201101 (2020).
[78] S. Datta, M. Saleem, K. G. Arun, and B. S. Sathyaprakash, Phys. Rev. D **109**, 044036 (2024).
[79] S. Datta, arXiv:2303.04399.
[80] Q. Hu and J. Veitch, Astrophys. J. **945**, 103 (2023).
[81] C. K. Mishra, K. G. Arun, B. R. Iyer, and B. S. Sathyaprakash, Phys. Rev. D **82**, 064010 (2010).
[82] C. M. Will and N. Yunes, Classical Quantum Gravity **21**, 4367 (2004).
[83] M. Tse *et al.*, Phys. Rev. Lett. **123**, 231107 (2019).
[84] B. P. Abbott *et al.* (KAGRA, LIGO Scientific, and Virgo Collaborations), Living Rev. Relativity **21**, 3 (2018).
[85] F. Acernese *et al.* (Virgo Collaboration), Classical Quantum Gravity **32**, 024001 (2015).
[86] T. Akutsu *et al.* (KAGRA Collaboration), Prog. Theor. Exp. Phys. **2021**, 05A102 (2021).
[87] H. Luck *et al.*, J. Phys. Conf. Ser. **228**, 012012 (2010).
[88] B. Iyer *et al.*, Technical Report No. LIGO-M1100296-v2, 2011.
[89] M. Saleem *et al.*, Classical Quantum Gravity **39**, 025004 (2022).
[90] T. Damour, B. R. Iyer, and B. S. Sathyaprakash, Phys. Rev. D **62**, 084036 (2000).
[91] C. Cutler and E. E. Flanagan, Phys. Rev. D **49**, 2658 (1994).
[92] K. Thorne, Rev. Mod. Phys. **52**, 299 (1980).
[93] L. Blanchet and T. Damour, Phys. Rev. D **46**, 4304 (1992).
[94] D. Christodoulou, Phys. Rev. Lett. **67**, 1486 (1991).
[95] K. Thorne, Phys. Rev. D **45**, 520 (1992).
[96] K. G. Arun, L. Blanchet, B. R. Iyer, and M. S. S. Qusailah, Classical Quantum Gravity **21**, 3771 (2004); **22**, 3115(E) (2005).
[97] L. Blanchet, Classical Quantum Gravity **15**, 89 (1998).
[98] S. Foffa and R. Sturani, Phys. Rev. D **101**, 064033 (2020).
[99] B. P. Abbott *et al.* (LIGO Scientific and Virgo Collaborations), Phys. Rev. Lett. **116**, 221101 (2016); **121**, 129902(E) (2018).
[100] H. Cramer, *Mathematical Methods in Statistics* (Pergamon Press, Princeton University Press, NJ, 1946).
[101] C. Rao, Bull. Calcutta Math. Soc. **37**, 81 (1945).

[102] C. Helström, *Statistical Theory of Signal Detection*, 2nd ed., International Series of Monographs in Electronics and Instrumentation Vol. 9 (Pergamon Press, Oxford, UK, New York, U.S.A., 1968).
[103] E. Poisson and C. M. Will, Phys. Rev. D **52**, 848 (1995).
[104] F. Pretorius, arXiv:0710.1338.
[105] P. Ajith *et al.*, Classical Quantum Gravity **24**, S689 (2007).
[106] S. Khan, S. Husa, M. Hannam, F. Ohme, M. Pürrer, X. Jiménez Forteza, and A. Bohé, Phys. Rev. D **93**, 044007 (2016).
[107] G. Pratten, S. Husa, C. Garcia-Quiros, M. Colleoni, A. Ramos-Buades, H. Estelles, and R. Jaume, Phys. Rev. D **102**, 064001 (2020).
[108] S. Khan, K. Chatziioannou, M. Hannam, and F. Ohme, Phys. Rev. D **100**, 024059 (2019).
[109] G. Pratten *et al.*, Phys. Rev. D **103**, 104056 (2021).
[110] C. García-Quirós, M. Colleoni, S. Husa, H. Estellés, G. Pratten, A. Ramos-Buades, M. Mateu-Lucena, and R. Jaume, Phys. Rev. D **102**, 064002 (2020).
[111] A. Pai and K. Arun, Classical Quantum Gravity **30**, 025011 (2013).
[112] S. Datta, A. Gupta, S. Kastha, K. G. Arun, and B. S. Sathyaprakash, Phys. Rev. D **103**, 024036 (2021).
[113] M. Saleem, S. Datta, K. G. Arun, and B. S. Sathyaprakash, Phys. Rev. D **105**, 084062 (2022).
[114] L. Finn and D. Chernoff, Phys. Rev. D **47**, 2198 (1993).
[115] T. Robson, N. J. Cornish, and C. Liu, Classical Quantum Gravity **36**, 105011 (2019).
[116] S. Babak, J. Gair, A. Sesana, E. Barausse, C. F. Sopuerta, C. P. L. Berry, E. Berti, P. Amaro-Seoane, A. Petiteau, and A. Klein, Phys. Rev. D **95**, 103012 (2017).
[117] M. Vallisneri, Phys. Rev. D **77**, 042001 (2008).
[118] U. Dupletsa, J. Harms, K. K. Y. Ng, J. Tissino, F. Santoliquido, and A. Cozzumbo, arXiv:2404.16103.
[119] P. Ajith, Phys. Rev. D **84**, 084037 (2011).
[120] S. Kastha, A. Gupta, K. G. Arun, B. S. Sathyaprakash, and C. Van Den Broeck, Phys. Rev. D **98**, 124033 (2018).
[121] S. Hild *et al.*, Classical Quantum Gravity **28**, 094013 (2011).
[122] A. Mangiagli, A. Klein, M. Bonetti, M. L. Katz, A. Sesana, M. Volonteri, M. Colpi, S. Marsat, and S. Babak, Phys. Rev. D **102**, 084056 (2020).
[123] E. Berti, A. Buonanno, and C. M. Will, Phys. Rev. D **71**, 084025 (2005).
[124] P. A. R. Ade *et al.* (Planck Collaboration), Astron. Astrophys. **594**, A13 (2016).
[125] B. P. Abbott *et al.* (LIGO Scientific and Virgo Collaborations), Phys. Rev. Lett. **116**, 061102 (2016).
[126] B. P. Abbott *et al.* (LIGO Scientific and Virgo Collaborations), Phys. Rev. Lett. **116**, 241103 (2016).
[127] B. P. Abbott *et al.* (LIGO Scientific and Virgo Collaborations), Phys. Rev. X **9**, 031040 (2019).
[128] W. Del Pozzo, J. Veitch, and A. Vecchio, Phys. Rev. D **83**, 082002 (2011).
[129] B. P. Abbott *et al.* (LIGO Scientific and Virgo Collaborations), Phys. Rev. D **100**, 104036 (2019).
[130] R. Abbott *et al.* (LIGO Scientific and Virgo Collaborations), Phys. Rev. D **103**, 122002 (2021).
[131] M. Isi, K. Chatziioannou, and W. M. Farr, Phys. Rev. Lett. **123**, 121101 (2019).
[132] I. Gupta *et al.*, CE Document No. P2300019-v2, 2023.